Predicted current densities in the brain during transcranial electrical stimulation

R. N. Holdefer[a*], **R. Sadleir**[b], and **M. J. Russell**[a,c]

a*Active Diagnostics, Inc. Davis, CA 95616, USA*

b*Department of Biomedical Engineering, University of Florida, Gainesville, FL 32611, USA*

c*Aaken Laboratories, Inc., Davis, CA 95616, USA*

Abstract

Objective—We sought an electrical modeling approach to evaluate the potential application of finite element method (FEM) modeling to predict current pathways and intensities in the brain after transcranial electrical stimulation.

Methods—A single coronal MRI section through the head, including motor cortex, was modeled using FEM. White matter compartments with both anatomically realistic anisotropies in resistivity and with a homogeneous resistivity were modeled. Current densities in the brain were predicted for electrode sites on the scalp and after theoretical application of a conductive head restraint device.

Results—Localized current densities were predicted for the model with white matter anisotropies. Differences in predicted peak current densities were related to location of stimulation sites relative to deep sulci in the brain and scalp shunting that was predicted to increase with inter-electrode proximity. A conductive head restraint device was predicted to shunt current away from the brain when a constant current source was used.

Conclusions—The complex geometry of different tissue compartments in the head and their contrasting resistivities may jointly determine the strength and location of current densities in the brain after transcranial stimulation. This might be predictable with FEM incorporating white matter anisotropies. Conductive head restraint devices during surgery may be contraindicated with constant current stimulation.

Significance—Individually optimized tcMEP monitoring and localized transcranial activation in the brain might be possible through FEM modeling.

1. Introduction

Transcranial electrical stimulation to elicit motor evoked potentials (tcMEPs) has become the primary means of selectively assessing the integrity of the motor pathways during spinal cord surgery. Typically, these potential are elicited by placing subdermal electrodes in the scalp at locations intended to excite motor pathways. A short train of electrical pulses is then used to elicit potentials that are recorded from muscles of the upper or lower limbs. The pulses used

*Corresponding author. Address: Neurological Monitoring Associates, 5464 North Port Washington Road, P.O. Box 17900, MS #173, Milwaukee, WI 53217, USA. Tel.: +1 414 351 6666; fax: +1 414 351 6999., *E-mail address*: rholdefer@yahoo.com (R.N. Holdefer).

for this procedure are of short duration (50–500 µs) but high voltage (100–200 V) (Bose et al., 2004; Calancie et al., 2001; Haghighi and Zhang, 2004; MacDonald et al., 2003; Pelosi et al., 2002; Zentner, 1989). The use of tcMEPs has become the standard of care in many types of spinal and brain surgery.

Despite its value in mitigating motor deficits, tcMEP monitoring encounters two significant challenges. First, systemic variables (e.g. anesthetic agents, blood pressure, etc.) affecting this signal must be distinguished from those directly associated with the surgical procedure with the potential for injury and damage. Several techniques for identifying and managing these systemic changes have been described (e.g. Calancie et al., 1998; Chen, 2004; MacDonald et al., 2003; Pechstein et al., 1998; Pelosi et al., 2001). Second, even under favorable anesthetic regimens and stable systemic variables, obtaining tcMEPs of sufficient amplitude and localization can require trial and error testing of parameters such as stimulus train length, inter-stimulus interval, stimulus intensity and electrode location.

Reports of the most effective tcMEP electrode locations have varied. Sites corresponding to the International 10/20 System at C1/C2 or C3/C4 are favored because of their assumed proximity to the leg or arm representation in motor cortex. Locations a few centimeters anterior to these have been reported (Deletis, 2002; Neuloh and Schramm, 2002; Pelosi et al., 2001), as have midline sites (Kothbauer, 2002; Langeloo et al., 2003). These difference in electrode locations reflect the desired target area for tcMEP recording during surgical monitoring (e.g. upper or lower limbs).

In addition, optimal stimulation sites may vary with individual differences in the skull or brain compartment of the head. Clearly, the geometry and resistivities of the various tissue compartment of the head determine current pathways in the brain (Haueisen et al., 1997; Laarne et al., 1999; Nadeem et al., 2003), and could potentially contribute to the variability seen from patient to patient in optimal tcMEP stimulation parameters. Given the long history of attempts to model current flow within the head for the analysis of electroencephalographic (EEG) recordings (e.g. Ary et al., 1981; Schneider, 1974), the use of electrical modeling to better understand and control current pathways in the brain after tcMEP seems a natural extension.

Many recent electrical models of the head are simplified 3 or 4 compartment models, which include the scalp, skull, and brain (or gray and white matter) (Benar and Gotman, 2002; Clay and Ferree, 2002; Goncalves et al., 2003; Kowalski et al., 2002; Seilwinder et al., 2002). The effects of the anisotropic resistivity of white matter fiber tracts, (white matter resistivity varies by close to an order of magnitude with the direction of current flow) have not been explored. In this study, we model current pathways in an anatomically realistic section through the head and motor cortex, which includes modeling of white matter anisotropies. The potential utility of an electrical modeling approach to better understanding and predicting current densities in the brain during transcranial electrical stimulation is demonstrated, specifically as it regards different stimulation sites on the head and external head restraint devices used during surgery.

2. Methods

2.1. Modeling current density

Current density calculations were derived from a FEM model of a coronal MRI section (6.5 mm slice thickness) through the upper limb motor cortex of one of the authors (MRJ). Modeling proceeded in four steps:

1. segmentation to identify tissue compartment boundaries

2. assignment of resistivities to tissue compartments

3. assignment of stimulation sites and intensities

4. application of voltage or current boundary conditions

Finite element 2D modeling was performed using FEMLAB 3.1 software are (Comsol, Burlington MA).

2.1.1. Segmentation—The scanned film image (Fig. 1A) was contrast-enhanced, and then preliminary tissue compartment boundaries were identified automatically on the basis of grayscale values with commercially available software (Canvas7, ACD Systems, Inc.). These preliminary boundaries were then superimposed over the original MRI scan, and final identification, or segmentation, of tissue compartments was done by hand. The segmented tissue boundaries for the MRI scan are shown in Fig. 1B. Matching MRI and anatomical sections from the human brain atlases of Talairach and Tournoux, and Schaltenbran and Wahren (Nowinski et al., 1997) greatly aided in identifying gray matter compartments, particularly deep brain nuclei.

To illustrate external factors influencing tcMEPs, a Gardner-Wells tongs (a metal frame that is often attached to the patient's head during cervical surgeries) was included as a separate subdomain in subsequent models. Both insulated and non-insulated tongs were modeled.

2.1.2. Resistivities—Fig. 1B lists the resistivity of the tissue compartments used in the segmented model. Most tissue resistivity estimates were taken from Haueisen et al. (1997), which summarized resistivity values from many studies and provided mean values for tissue compartments. The exception was for white matter resistivity, which varies with fiber orientation (Geddes and Baker, 1967). A single resistivity was assigned to the white matter compartment in some of our models for comparison with previous FEM studies (e.g. Haueisen et al., 1997;Nadeem et al., 2003). In other models, a more accurate representation was obtained by assigning resistivity to white matter elements on the basis of fiber orientation. To accomplish this, a grid was placed over the white matter compartment (Fig. 1A), and the dominant fiber orientation in each square (element) was determined. Fiber orientations in elements, which included the internal capsule, corpus callosum, and the necks of narrow gyri were readily assigned. For other areas the dominant fiber orientations were estimated from gross anatomical dissections (Berry et al., 1995). Conductivity in the **i**th element was specified by the tensor

$$\sigma_i = \mathbf{R}_z^T \mathbf{W} \mathbf{R}_z$$

where the rotation matrix $\mathbf{R_z}$ was

$$\mathbf{R_z} = \left[\begin{array}{cc} \cos(\alpha) & -\sin(\alpha) \\ \sin(\alpha) & \cos(\alpha) \end{array} \right],$$

α is the fiber orientation angle with respect to the model *x*-axis, and

$$\mathbf{W} = \left[\begin{array}{cc} 1/r_l & 0 \\ 0 & 1/r_t \end{array} \right]$$

was a matrix containing diagonal entries consisting of the reciprocal longitudinal (r_l) and transverse (r_t) resistivities. Values of r_l and r_t were chosen to be 85 and 800 Ωcm, respectively, (Geddes and Baker, 1967).

2.1.3. Stimulation sites and intensities—Electrodes were placed at sites commonly used for tcMEP (C1/C2 and C3/C4, International 10/20 System). Electrodes were also modeled over the deep sulci of motor cortex representing the upper limbs and the lateral sulci, with the hypothesis that low resistivity CSF in these sulci would serve as a preferential current pathway. Stimulation intensity was ±50 V, using a constant voltage source. Although, constant voltage

devices are most commonly used for tcMEP, a constant current source (15 mA) was used for models, which included head restraint devices, with electrodes over the motor cortical sulci. Constant current sources are also used for tcMEP (e.g. Novak et al., 2004; Zhou and Kelly, 2001), and unlike constant voltage devices pose potential problems with current shunting when used in proximity to metallic, head restraint devices (Moller, 1995). A DC model of stimulation was used, so the effects of different pulse durations were not investigated in this study.

2.1.4. Application of boundary conditions—Current densities (A/m) within the segments resulting from bilateral electrode stimulations (±50 V) were calculated in the segmented slice, using the finite element model generated by FEMLAB. Finite element modeling was used because it can suitably represent geometrically complex compartments and anisotropic (i.e. different values in different directions) electrical properties of tissues such as nerves. The full details are contained in the FEMLAB manual (Comsol, 2004). In brief, a mesh was constructed by first detecting edge contours of each segment within the image, then converting the region within each contour into 2D subdomains. Meshing of the entire structure was carried out using standard FEMLAB meshing routines, requiring that minimum element quality (q) be 0.1. Triangle q is given by the formula

$$q = \frac{4\sqrt{3}a}{h_1^2 + h_2^2 + h_3^2}$$

where a is the triangle area and h_1, h_2, h_3 are the side lengths of the triangle. q is a number between 0 and 1. If $q > 0.6$, the triangle is of acceptable quality, and $q = 1$ when $h_1 = h_2 = h_3$. If triangle elements have low q they are typically long and thin, which may result in the solution on the mesh being inaccurate. The modal value of mesh quality (q) in our mesh was 0.98. Current densities were then calculated from the forward solution of Laplaces equation on the elements of this mesh.

Linear meshes for models contained around 150,000 elements and 310,000 degrees of freedom. Solution of the models was performed to a relative precision of less than 1×10^{-6}, using LU decomposition and back substitution The results were presented either as current streamline plots, as seen in Fig. 5, or as current density shading plots in Fig. 2–Fig. 4 and Fig. 6.

3. Results

Results of our FEM investigation of transcranial stimulation effects are shown in Fig. 2–Fig. 6. In Fig. 2, the effects of resistivity variations on current densities are examined, with particular attention to white matter anisotropies. Current densities were obtained for sections indicated by the line segments in Fig. 2A–C, and plotted in Fig. 2D. These sections are through portions of white matter, which include corticospinal fibers. Because of the large range of current densities the colors were set at a linear scale with upper and lower limits to facilitate visualization of relative current densities achieved in the brain. Effective current intensities needed for microstimulation of motor cortex were used as a rough guide to setting the upper and lower and limits of these plots (e.g. Cheney et al., 1985).

In Fig. 2A, white matter was modeled as a single, homogeneous compartment with a resistivity for current pathways across fiber tracts (800 Ωcm Geddes and Baker, 1967). As expected, much of the current was shunted between the electrodes and through the scalp. Current densities for the section through white matter of this model were relatively low (<10 A/m) and uniform (Fig. 2D). In Fig. 2B, white matter was modeled as a homogenous compartment with a resistivity for current pathways parallel to fiber tracts (85 Ωcm; Geddes and Baker, 1967). This 'along fiber' resistivity resulted in significant current densities in the crowns of gyri underneath the stimulation sites (arrows) Relatively high densities were also present throughout much of

the white matter (>50 A/m), and were greatest in the neck region of cortical gyri (Fig. 2D), possibly due to low resistivity white matter in these necks acting as a current sink. In contrast, localized current densities were observed in the more realistic representation of the white matter, which included elements whose resistivity varied depending on the dominant fiber orientation (Fig. 2C). A localized current density peak of 49 A/m was observed in the section through white matter of this model (Fig. 2D), as well as relatively high current densities in the crowns of more medial gyri.

In Fig. 3, the effects of changing skull resistivity on predicted current densities in the model with white matter anisotropies (Fig. 2C) were investigated. In Fig. 3A, the more commonly cited and higher resistivity of 23,809 Ω cm (Rush and Driscoll, 1968) was used, and in Fig. 3B a value of 6493 Ω cm was used from a study which included in vivo measurements (Oostendorp et al., 2000). Although, compact and cancellous bone is shown in the plots, current densities were calculated using a single resistivity for the skull (either 23,809 or 6493 Ω cm). Fig. 3C plots the current densities for a section through the white matter of these two models, and also for the model in Fig. 2C which included both compact and cancellous bone (16,000 and 2500 Ω cm, respectively). Unlike the different white matter representations shown in Fig. 2, difference in skull resistivity uniformly changed the magnitude while yielding a similar localization of current densities in the brain. This was seen in the simple shift of the curve along the *y*-axis in Fig. 3C which illustrated the anticipated inverse relationship between current density and skull resistivity.

Variations in electrode locations for the model incorporating white matter anisotropies (Fig. 2C) are shown in Fig. 4. Panels are arranged with increasing distance between electrode sites from Fig. 4A–D. As a relative measure of current shunting through the scalp between the electrodes, current densities were determined for the scalp midway between the stimulation sites. As expected, current densities in the scalp were greatest when stimulation was at the C1 and C2 sites (Fig. 4A, >300 A/m) and decreased with increased distance between electrodes to 40 and 50 A/m for the sites over the lateral sulci (Fig. 4D). These changes in current densities with distance between stimulation sites are seen in Fig. 4D and not the other panels because the scalp currents in Fig. 4A–C exceeded the upper limit of the color scale (50 A/m).

Higher current densities in the brain were associated with decreased current shunting between the electrodes through the scalp. Peak current densities were determined for a small area of white matter expected to include axons carrying motor commands to the arms and face, indicated by the bolded circles in Fig. 4. Current densities ranged from a peak of 40 A/m for the C1 an and C2 stimulation on sites (Fig. 4A), to 89 A/m for the stimulation sites over the lateral sulci (Fig. 4D). Interestingly, current densities were comparable for the C3 and C4 sites and the deep sulci sites (70–80 A/m), despite the greater scalp shunting in the latter. Possibly, the relatively high currents seen in the median fissure for the deep sulci sites (Fig. 4B) contributed to the densities observed in the white matter carrying motor cortical axons (bolded circles), and compensated in part for the current lost through the scalp.

An illustration of current pathways through the model with deep sulci stimulation sites and white matter anisotropies (Fig. 2C and Fig. 4B) is shown in Fig. 5. Only 300 pathways are plotted for readability. As the number of plotted pathways increases, differences in the number of lines within a circumscribed area increasingly corresponds to relative differences in current densities. Some of the current pathways, for example those through low-resistivity scalp and CSF, are as expected. Most are more complicated, being jointly determined by contrasts in resistivity between the 8 different tissue compartments and white matter anisotropies.

Fig. 6 shows a model with a Gardner-Wells tongs, a metal head restraint device used to apply traction during cervical surgeries. These stainless steel, conductive tongs are applied to the

head a few centimeters from the stimulation sites at C3 and C4 commonly used for tcMEP in intraoperative monitoring. The model with white matter anisotropies and deep sulci stimulation sites (Fig. 2C and Fig. 4B) was used except with the addition of a non-conducting tongs (Fig. 6A) and the Gardner-Wells tongs (Fig. 6B) with a stainless steel resistivity. A constant current source (15 mA) was used in these cases, rather than the constant voltage sources used in the models shown in Fig. 2–Fig. 5. In both plots of Fig. 6, the current density distribution is displayed using a log scale. As expected, current was shunted through the Gardner–Wells tongs in Fig. 6B. Current densities in the gyri and sulci directly beneath the stimulation sites are orders of magnitude smaller when compared with the model with non-conducting tongs (Fig. 6A).

4. Discussion

To our knowledge, this study is the first to describe models with a realistic white matter compartment with elements whose resistivities vary with dominant fiber orientation. White matter resistivity along fibers is an order of magnitude less than across fibers. This 'along fiber' current pathway resulted in a topology with some relatively high and circumscribed current densities compared to the models with a homogeneous white matter resistivity. Relatively high current densities were predicted for small areas of white matter expected to include axons from the upper limb motor cortex.

Current density in white matter representing the arms and face was also related to the distance between stimulation sites, and their location on the modeled coronal section. For closely spaced stimulation sites at C1 and C2, more current was shunted through the scalp and away from the brain as compared to more widely spaced sites located over the lateral sulci. In addition, location of electrodes over deep sulci determined current densities. The model predicted preferential current pathways for low resistivity CSF in these sulci, drawing current into the brain and to the crowns of narrow gyri bounded on both sides by the sulci. A key point emerging from this modeling is that if the detailed head anatomy is known, judicious placement of electrodes and use of low stimulation intensities may result in highly specific activation of selected areas of the brain.

Our modeling results also have relevance to the physiological mechanisms utilized by tcMEP stimulation. Previous research has suggested the site of activation for low intensity stimulation is the initial segment of motor cortical pyramidal cells which contribute descending fibers to the cord, while at higher intensities the axons some distance from the cell body are activated (Amassian, 2002). It is well established that the initial axon segment has the lowest threshold for generation of an action potential. However, the FEM modeling suggests that at low stimulation intensities small areas in white matter may be activated first, depending on the dominant fiber orientation. Peak current densities in these areas of white matter could significantly exceed those of the motor cortical area projecting through them.

4.1. FEM modeling and individual differences

Accurate prediction in electrical models of the head for use in surgery will also require incorporation of individual differences in these models. These differences are clearest for the skull compartment. For example, the presence of the highly vascularized anterior fontanel in young children is a lesser barrier to current flow than bone, because of its much lower resistivity (scalp: 230 Ωcm; blood: 160 Ωcm; bone 7560 Ωcm). There are large differences in fontanel size and time of closure between and within races with two thirds of Nigerian neonates (Adeyemo and Omotade, 1999) having larger fontanels than the upper limit reported for white American neonates (Popich and Smith, 1972). These large skull openings substantially distort the propagation of current from within the head (Flemming et al., 2005; Heasman et al.,

2002) and it is likely that they have a similar effect on the propagation of signals from outside of the calvarium.

There are also significant difference for normal adults in the degree and timing of suture closing (Law, 1993). These differences greatly affect the conductivities of the bone (Akhtari et al., 2002), and may help to explain the observation that for some individuals limb activations are effectively obtained at C1 and C2, while for other patients these sites are ineffective. Midline sites (approximately Cz and 6 cm anterior to Cz) often can be used instead, presumably taking advantage of relatively low resistance current pathways at the sagittal suture (Deletis, 2002).

4.2. Electrical modeling of the coronal section

Although, the tissue compartments correspond closely with those in the MRI section used for segmentation, several limitations should be mentioned. The thickness of compact bone was inferred since it is dimly represented in an MRI. In addition, boundaries between gray and white matter often were not clearly demarcated in the MRI. For this reason, matching sections from the human brain atlases of Talairach and Tournoux, and Schaltenbrand (Nowinski et al., 1997) were consulted for the thickness of neocortex, and location of deep brain nuclei. Blood vessels were not included in the model, but they are only likely to be important if they are close to the stimulation site (Haueisen et al., 1997). Also, we were necessarily limited to fiber orientation in the plane of the modeled coronal section. Fiber tracts outside of this plane (e.g. in a sagittal plane) were not represented and would conduct current away from the section. This would be expected to change the localization of current densities in the brain, and emphasizes the importance of extending this modeling to a full, 3D electrical model of the head, which includes white matter anisotropies in resistivity.

Many of the tissue resistivity values were from older studies and vary over a wide range. For this reason we chose to use averages compiled from many of these studies, as summarized in Haueisen et al. (1997). Also, in many cases, resistivity values were from in vitro measurements, and their applicability to living tissue is unclear. Skull resistivity measurements, which are crucial for accurate FEM modeling of the head, appear to be on more favorable ground. There is now general agreement between recent in vivo and in vitro reports on its values (Ferree et al., 2000; Goncalves et al., 2003, Law, 1993; Oostendorp et al., 2000). These skull resistivity measurements are significantly lower than those from an older study (Rush and Driscoll, 1968). Different skull resistivities were investigated in the present study, along with a representation of skull, which included separate resistivity compartments of cancellous and compact bone. These different representations of the skull in the model changed the overall magnitude of current densities in the brain, but largely preserved the topography of their localization.

Of course, current paths from transcranial stimulation in the operating room are a 3D phenomenon, and a complete model would require an accurate 3D model of the head. A recent report by Nadeem et al. (2003) used such a model to predict currents in the brain using simulated transcranial magnetic stimulation and electroconvulsive therapy. However, we have limited ourselves to a few generalizations relative to the preferential current pathways offered by optimally oriented fiber pathways in white matter and CSF in deep sulci. To the extent that these structures persist across many sections, similar effects will be seen in a 3D head model.

4.3. Practical application to surgical monitoring

Our modeling results suggest that the most effective sites on the scalp for transcranial stimulation may not necessarily be directly over the desired target in the brain. Instead, points over deep sulci adjacent to a brain target may 'focus' current and result in higher current densities at the desired location. In addition, with increasing proximity of stimulation sites,

current shunting through the scalp may increase at the expense of current densities in the brain. Thus, for some brain targets a trade-off might exist between adequate separation between electrodes to minimize scalp currents, and location of electrodes over the targets. With further development, it seems possible that FEM could eventually guide electrode placement for individually optimized tcMEP monitoring and more localized brain activation to minimize patient movements during stimulation.

The results also suggest that the use of externally applied devices such as the Gardner–Wells tongs may be problematic if they are made out of conductive materials. For a constant current device, the modeling predicted current shunting through the metal tongs, reducing current densities in the brain directly beneath the electrodes by several orders of magnitude. Electrical insulation of the tongs would eliminate these difficulties. Wilson frames are conducting metal devices also used for head restraint and traction in surgery, but they can be purchased with either insulated or steel traction pins. Wilson frames used with electrically insulated pins are expected to have little or no effect on electric currents.

Electrical modeling of the head should also find application improving tcMEP safety in the operating room. Electrical modeling can be used to predict not only the maximum charge load in the brain, but also its distribution. However, this would require a full electro-magnetic model rather than the electrostatic models which are commonly found in the literature.

5. Summary

Current pathways are determined by the complex geometry of the various tissue compartments of the head, and by contrasts in resistivities between these tissue compartments. The addition of white matter anisotropies in resistivity to our model resulted in a specific topography of current densities in the brain and illustrates the potential importance of these anisotropies for electrical modeling of the head. A trade-off may exist between positioning electrodes directly over a desired brain target and shunting of current through the scalp, which will be determined in part by the proximity of the electrodes. In as much as the results of this study were obtained from modeling a single coronal section through motor cortex, they must be regarded as preliminary. Future studies employing a full, 3D model raise the prospect of using anatomical features (e.g. deep sulci) in individualized, electrical head models to 'focus' current densities. This may make it possible to accurately target brain areas using transcortical stimulation while at the same time minimizing unwanted patient movements.

References

Adeyemo AA, Omotade OO. Variation in fontanel size with gestational age. Early Hum Dev 1999;54:207–214. [PubMed: 10321787]

Akhtari M, Bryant HC, Mamelak AN, Flynn ER, Heller L, Shih JJ, Mandelkern M, Matiachov A, Ranken DM, Best ED, DiMauro MA, Lee RR, Shutherling WW. Conductivities of three-layer live human skull. Brain Topogr 2002;14:151–167. [PubMed: 12002346]

Amassian, VE. Animal and human motor system neurophysiology related to intraoperative monitoring. In: Deletis, V.; Shels, J., editors. Neurophysiology in neurosurgery. Amsterdam: Academic Press; 2002. p. 3-23.

Ary JP, Klein SA, Fender DH. Location of sources of evoked scalp potentials: corrections for skull and scalp thicknesses. IEEE Trans Biomed Eng 1981;28:447–452. [PubMed: 7287042]

Benar CG, Gotman J. Modeling of post-surgical brain and skull defects in the EEG inverse problem with the boundary element model. Clin Neurophysiol 2002;113:48–56. [PubMed: 11801424]

Berry, MM.; Standring, SM.; Bannister, LH. Nervous system. In: Bannister, LH.; Berry, MM.; Collins, P.; Dyson, M.; Dussek, JE.; Ferguson, MWJ., editors. Gray's anatomy. The anatomical basis of medicine and surgery. New York: Churchill Livingstone; 1995. p. 1191

Bose B, Sestokas AK, Swartz DM. Neurophysiological monitoring of spinal cord function during instrumented anterior cervical fusion. Spine J 2004;4:202–207. [PubMed: 15016399]

Calancie B, Harris W, Broton JG, Alexeeva N, Green BA. 'Threshold-level' multipulse transcranial electrical stimulation of motor cortex for intraoperative monitoring of spinal motor tracts: description of method and comparison to somatosensory evoked potential monitoring. J Neurosurg 1998;88:457–470. [PubMed: 9488299]

Calancie B, Harris W, Brindle F, Green BA, Landy HJ. Threshold-level repetitive transcranial electrical stimulation for intraoperative monitoring of central motor conduction. J Neurosurg 2001;95:161–168. [PubMed: 11599831]

Chen Z. The effects of isoflurane and propofol on intraoperative neurophysiological monitoring during spinal surgery. J Clin Monit Comput 2004;18:303–308. [PubMed: 15779842]

Cheney PD, Fetz EE, Palmer SS. Patterns of facilitation and suppression of antagonist forelimb muscles from motor cortex sites in the awake monkey. J Neurophysiol 1985;53:805–820. [PubMed: 2984355]

Clay MT, Ferree TC. Weighted regularization in electrical impedance tomography with applications to acute cerebral stroke. IEEE Trans Med Imaging 2002;21:629–637. [PubMed: 12166859]

Comsol, AB. FEMLAB user's guide v. 3.0. Burlington, MA: Comsol Inc.; 2004.

Deletis, V. Intraoperative neurophysiology and methodologies used to monitor the functional integrity of the motor system. In: Deletis, V.; Shels, J., editors. Neurophysiology in neurosurgery. Amsterdam: Academic Press; 2002. p. 25-51.

Ferree TC, Eriksen KJ, Tucker DM. Regional head tissue conductivity estimation for improved EEG analysis. IEEE Trans Biomed Eng 2000;47:1584–1592. [PubMed: 11125593]

Flemming L, Wang Y, Caprihan A, Eiselt M, Hauseisen J, Okeda Y. Evaluation of the distortion of EEG signals caused by a hole in the skull mimicking the fontanel in the skull of human neonates. Clin Neurophysiol 2005;116:1141–1152. [PubMed: 15826855]

Geddes LA, Baker LE. The specific resistance of biological material—a compendium of data for the biomedical engineer and physiologist. Med Biol Eng 1967;1967:271–293. [PubMed: 6068939]

Goncalves SI, de Munck JC, Verbunt JPA, Bijma F, Heethaar RM, da Silva FH. *In vivo* measurement of the brain and skull resistivities using an EIT-based method and realistic models for the head. IEEE Trans Biomed Eng 2003;50:754–767. [PubMed: 12814242]

Haghighi SS, Zhang R. Activation of the external anal and urethral sphincter muscles by repetitive transcranial cortical stimulation during spine surgery. J Clin Monit Comput 2004;18:1–5. [PubMed: 15139577]

Haueisen J, Ramon C, Eiselt M, Brauer H, Nowak H. Influence of tissue resistivities on neuromagnetic fields and electric potentials studied with a finite element model of the head. IEEE Trans Biomed Eng 1997;44:727–735. [PubMed: 9254986]

Heasman BC, Valentin A, Alarcon G, Seoane JJG, Binnie CD, Guy CN. A hole in the skull distorts substantially the distribution of extracranial electrical fields in an in vitro model. J Clin Neurophysiol 2002;19:163–171. [PubMed: 11997728]

Kothbauer, KF. Motor evoked potential monitoring for intramedullary spinal cord tumor surgery. In: Deletis, V.; Shels, J., editors. Neurophysiology in neurosurgery. Amsterdam: Academic Press; 2002. p. 73-92.

Kowalski T, Silny J, Buchner H. Current density threshold for the stimulation of neurons in the motor cortex area. Bioelectromagnetics 2002;23:421–428. [PubMed: 12210560]

Laarne P, Kauppinen P, Hyttinen J, Malmivuo J, Eskola H. Effects of tissue resistivities on electroencephalogram sensitivity distribution. Med Biol Eng Comput 1999;37:555–559. [PubMed: 10723891]

Langeloo DD, Lelivelt A, Journee HL, Slappendel R, de Kleuver M. Transcranial electrical motor-evoked potential monitoring during surgery for spinal deformity. Spine 2003;28:1043–1050. [PubMed: 12768147]

Law SK. Thickness and resistivity variations over the upper surface of the human skull. Brain Topogr 1993;6:99–109. [PubMed: 8123431]

MacDonald DB, Zayed ZA, Khoudeir I, Stigsby B. Monitoring scoliosis surgery with combined multiple pulse transcranial electric motor and cortical somatosensory-evoked potentials from the lower and upper extremities. Spine 2003;28:194–203. [PubMed: 12544939]

Moller, AR. Intraoperative neurophysiologic monitoring. New York: Harwood; 1995.

Nadeem M, Thorlin T, Gandhi OP. Computation of electric and magnetic stimulation in human head using the 3-D impedance method. IEEE Trans Biomed Eng 2003;50:900–907. [PubMed: 12848358]

Neuloh, G.; Schramm, J. Intraoperative neurophysiological mapping and monitoring for supratentorial procedures. In: Deletis, V.; Shels, J., editors. Neurophysiology in neurosurgery. Amsterdam: Academic Press; 2002. p. 339-404.

Novak K, Bueno de Camargo A, Neuwirth M, Kothbauer K, Amassian VE, Deletis V. The refractory period of fast conducting corticospinal tract axons in man and its implications for intraoperative monitoring of motor evoked potentials. Clin Neurophysiol 2004;115:1931–1941. [PubMed: 15261873]

Nowinski, WL.; Bryan, RN.; Raghavan, R. Multiplanar navigation of the human brain. New York: Thieme; 1997. The electronic brain atlas.

Oostendorp TF, Delbeke J, Stegeman DF. The conductivity of the human skull: results of in vivo and in vitro measurements. IEEE Trans Biomed Eng 2000;47:1487–1492. [PubMed: 11077742]

Pechstein U, Nadstawek J, Zentner J, Schramm J. Isoflurane plus nitrous oxide versus propofol for recording of motor evoked potentials after high frequency repetitive electrical stimulation. Electroencephalogr Clin Neurophysiol 1998;108:175–181. [PubMed: 9566630]

Pelosi L, Stevenson M, Hobbs GJ, Jardine A, Webb JK. Intraoperative motor evoked potentials to transcranial electrical stimulation during two anaesthetic regimens. Clin Neurophysiol 2001;112:1076–1087. [PubMed: 11377268]

Pelosi L, Lamb J, Grevitt M, Mehdian SM, Webb JK, Blumhardt LD. Combined monitoring of motor and somatosensory evoked potentials in orthopaedic spinal surgery. Clin Neurophysiol 2002;113:1082–1091. [PubMed: 12088704]

Popich GA, Smith DW. Fontanelles: range of normal size. J Pediatr 1972:749–752. [PubMed: 5018385]

Rush S, Driscoll DA. Current distribution in the brain from surface electrodes. Anesth Analg 1968;47:717–723. [PubMed: 4972743]

Schneider M. Effect of inhomogeneities on surface signals coming from a cerebral dipole source. IEEE Trans Biomed Eng 1974;21:52–54. [PubMed: 4813877]

Seilwinder J, Kammer T, Andra W, Bellemann ME. A 3D FEM model for calculation of electromagnetic fields in transmagnetic stimulation. Biomed Tech (Berlin) 2002;47:285–288. [PubMed: 12451840]

Zentner J. Non-invasive motor evoked potential monitoring during neurosurgical operations on the spinal cord. Neurosurgery 1989;24:709–712. [PubMed: 2716979]

Zhou HH, Kelly PJ. Transcranial electrical motor evoked potential monitoring for brain tumor resection. Neurosurgery 2001;48:1075–1081. [PubMed: 11334274]
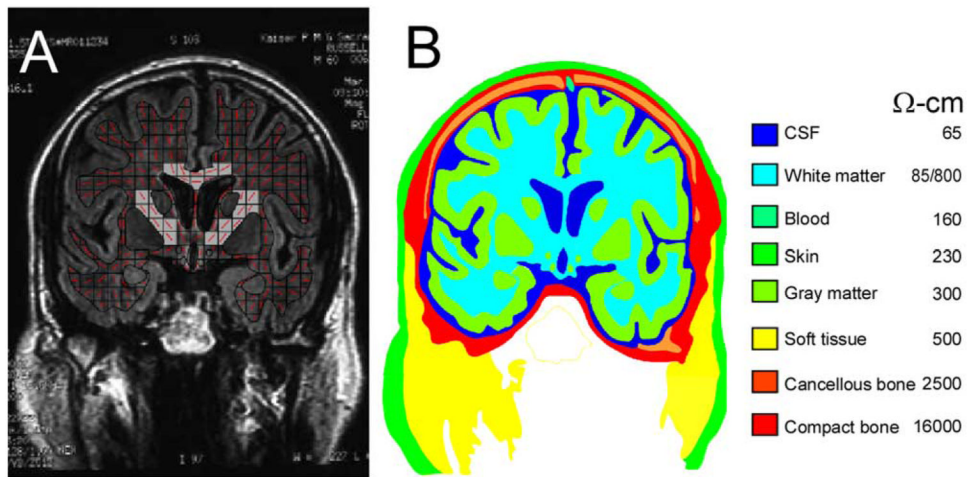
Fig. 1.
(A) An MRI coronal scan (6.5 mm) through the upper limb representation of motor cortex. Dominant fiber orientation is indicated by the red line segments in each square of a grid placed over the white matter compartment. Squares including the internal capsule and corpus callosum are shaded. (B) Segmentation of tissue compartments and their resistivities for the MRI scan shown in (A).
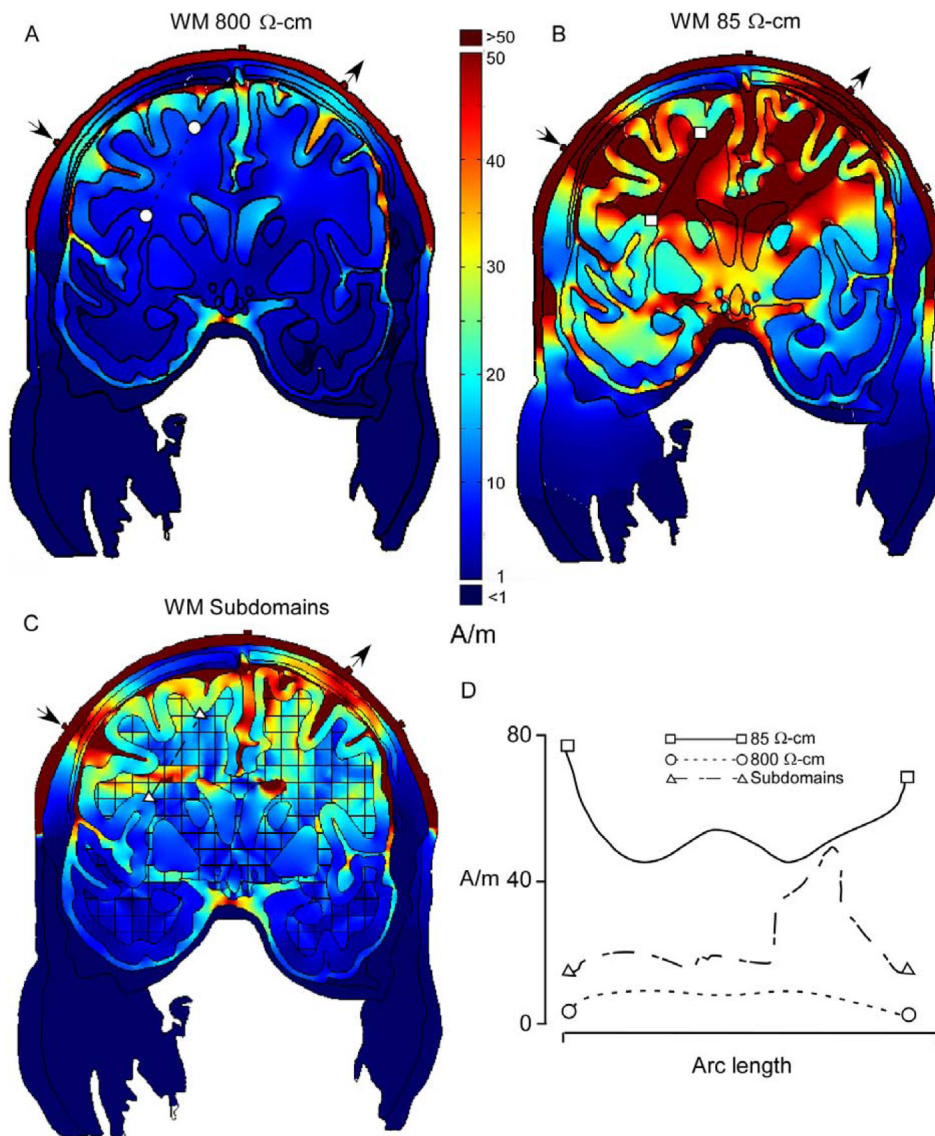
Fig. 2.
Current densities for the coronal section in Fig. 2, for models of current pathways across (A) 800 Ω cm, and parallel (B), 85 Ωcm, to white matter fiber tracts. (C) Model incorporating white matter anisotropies in resistivity. Resistivity was determined by dominant fiber orientation in each square of the grid. (D) Plots of current densities for sections (indicated by line segments) through white matter in (A), (B) and (C). Localization of current densities in white matter was greatest for the more realistic model in (C). Stimulation sites over the deep sulci are shown by the arrows.
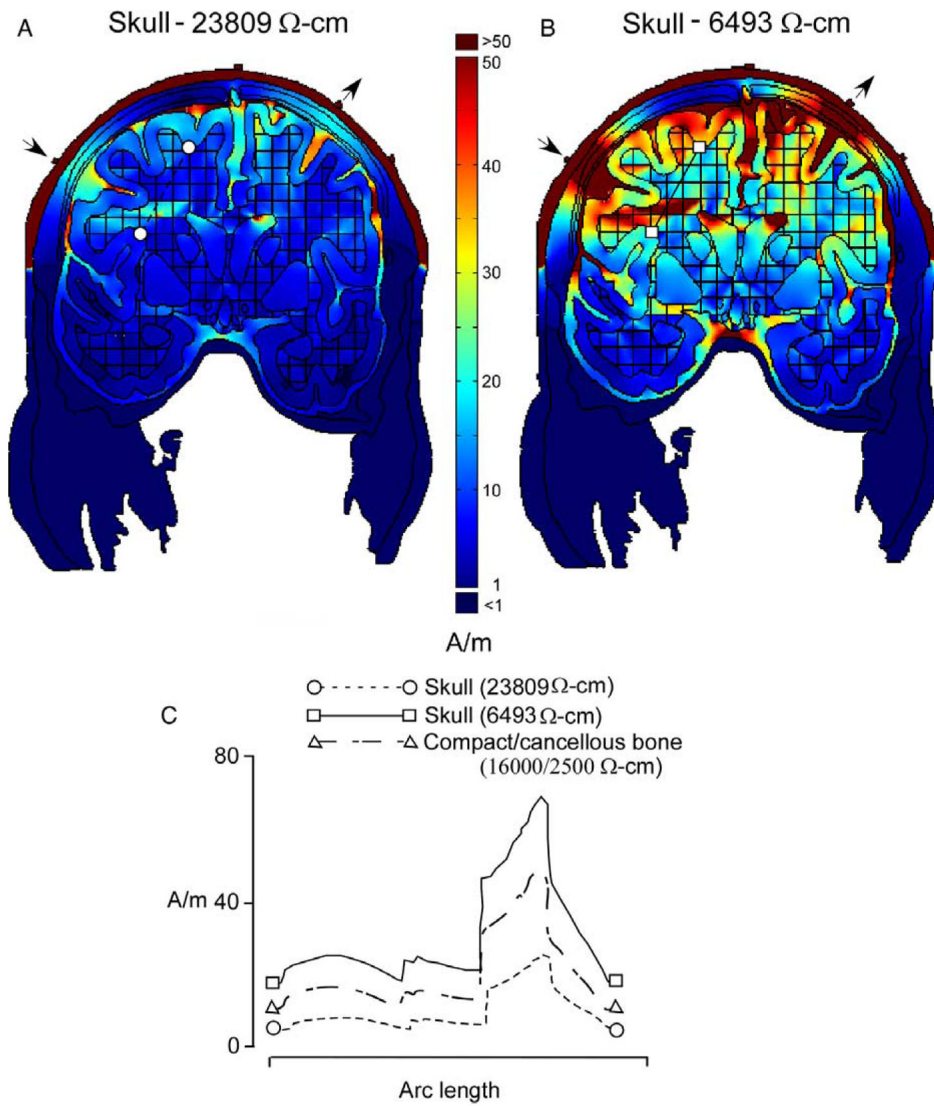
Fig. 3.
Current densities for models with skull resistivities of 23,809 Ωcm (A) and 6493 Ωcm (B). (C) Current density plots for sections indicated by line segments through white matter in (A) and (B), along with those for the model in Fig. 2C with white matter anisotropies. Decreasing skull resistivity increased current densities without changing their topography. Stimulation sites are shown by the arrows.
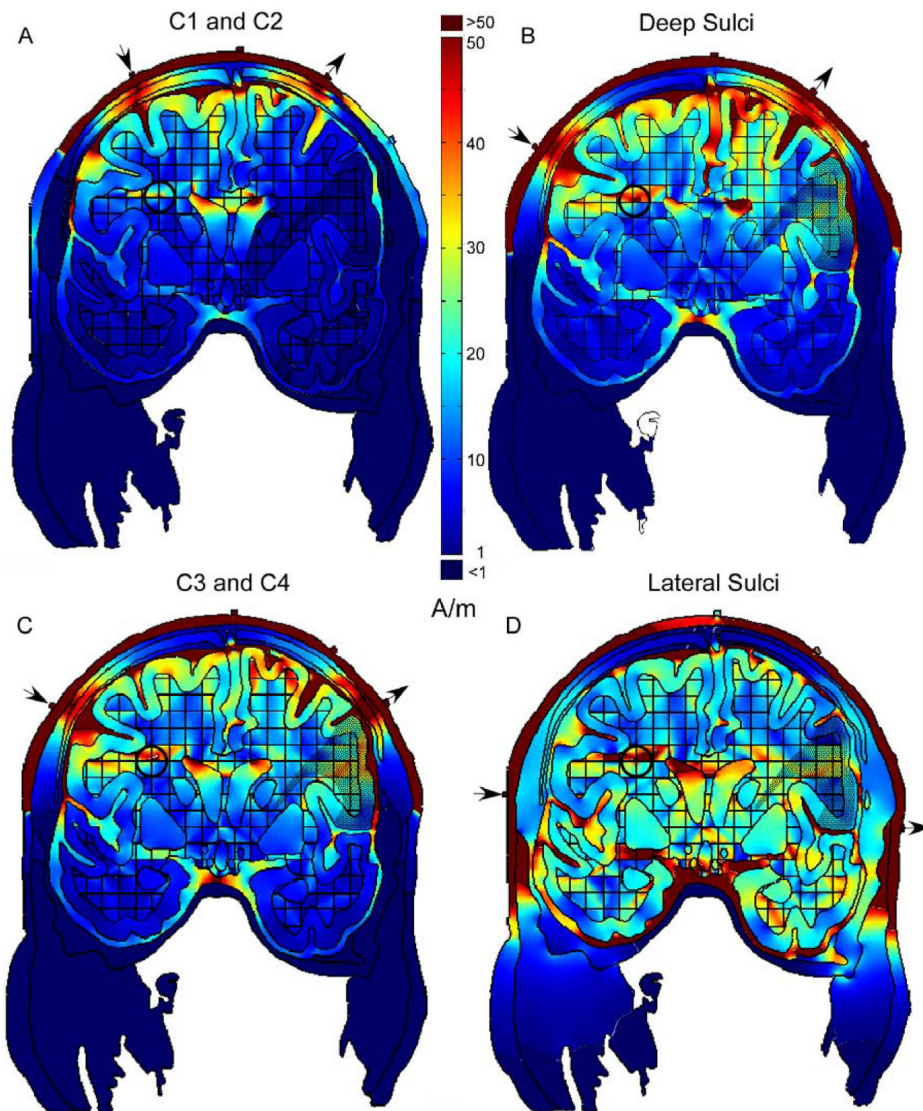
Fig. 4.
Panels (A)–(D) are arranged in order of increasing distance between stimulation sites on the scalp (arrows). Current densities in white matter representing the face and arms (circles) were lowest (40 A/m) for C1 and C2 stimulation sites (A) and highest (89 A/m) for the lateral sulci sites (D). In contrast, currents densities in the scalp between stimulation sites were greater in (A) as compared to (D). Gray and white matter representing the arms and face are indicated by the stippling on the right hand side of each model.
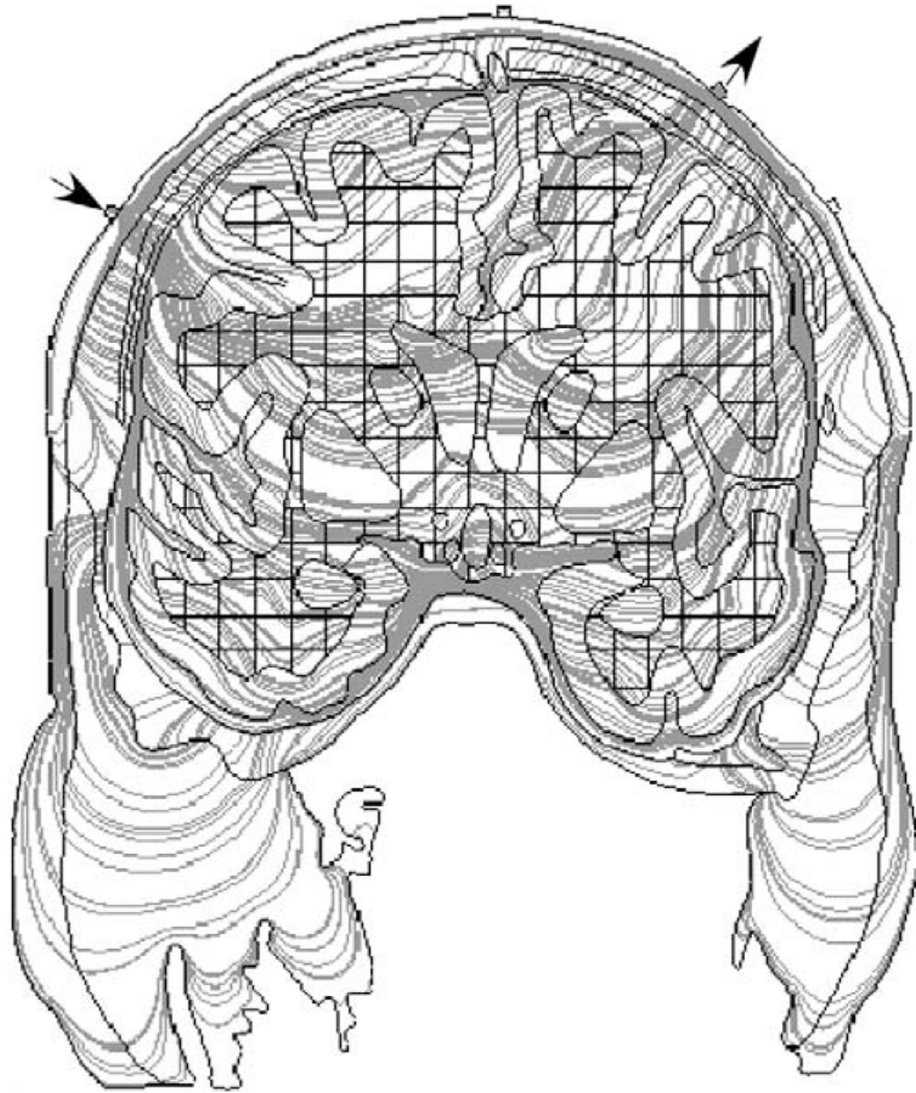
Fig. 5.
The gray lines are a plot of the current streamlines (the direction of the streamline at each point is determined by the relative values of the current density components J_x and J_y, respectively) through the head using the stimulation sites indicated by the arrows. Although they demonstrate the possible paths taken through the tissue, the current density plots in Fig. 4 provide a better indication of where stimulation is likely to occur.
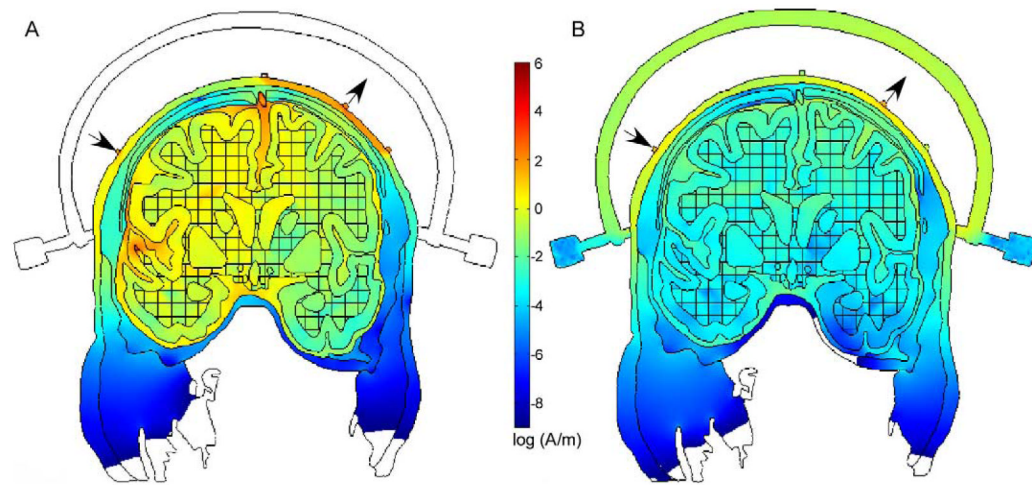
Fig. 6.
Modeled current densities with the addition of the Gardner–Wells tongs. (A) Tongs of high resistivity (>1 MΩ). (B) Current densities for a tongs with a resistivity for stainless steel, demonstrating current shunting through the tongs. A constant current stimulator was used.